Vision Research 165 (2019) 36–44

Contents lists available at ScienceDirect

Vision Research

journal homepage: www.elsevier.com/locate/visres

A millipede compound eye mediating low-resolution vision

John D. Kirwan*, Dan-E. Nilsson

Lund Vision Group, Department of Biology, Lund University, Sweden

ARTICLE INFO

Keywords:
Visual ecology
Visually-guided behaviour
Visual acuity
Photoreception
Myriapoda
Diplopoda

ABSTRACT

Millipedes are a species-rich and ancient arthropod clade which typically bear a pair of lateral compound eyes with a small number of large facets. To understand the visual tasks that underlie the evolution of millipede eyes, their spatial resolving performance is of key importance. We here investigate the spatial resolution of the millipede *Cylindroiulus punctatus* using behavioural assays. Individual animals were placed in the centre of a cylindrical arena under bright downwelling light, with dark stimuli of varying angular dimensions placed on the arena wall. We used continuous isoluminant stimuli based on a difference of Gaussians signal to test for orientation to the dark target via object taxis. Headings of individual animals were tracked in relation to the stimuli to determine whether the animals oriented towards the stimulus. We implemented a multilevel logistic regression model to identify the arc width of the stimulus that animals could resolve. We then modelled the angular sensitivity needed to identify this. We also related the visual performance to the 3D anatomy of the eye. We found that *C. punctatus* can resolve a stimulus of 56° period (sufficient to detect a 20° dark target). Assuming a contrast threshold of 10%, this requires a receptor acceptance angle of 72° or narrower. Spatial resolving power this low would only suffice for the simplest visual tasks, such as shelter-seeking.

1. Introduction

The evolutionary history of the myriapod clade (Myriapoda) has long been puzzling, not least with respect to their peculiar eyes. The visual ecology of Myriapoda, which comprises centipedes (Chilopoda), millipedes (Diplopoda) and the small eyeless paurapods and pseudocentipedes, has received little attention, compared to its sister clade, Pancrustacea (Regier et al., 2010; Rota-Stabelli et al., 2010). The myriapod compound eye typically comprises large, shallow ommatidia in several adjacent rows, formed from a cuticular lens abutting a shallow, wide microvillar rhabdom. Many groups are eyeless or have only reduced clusters of ocelli, as in members of the centipede genus *Scolopendra*. One centipede clade, the fast-moving Scutigeromorpha has a more sophisticated compound eye with many ommatidia, each with a crystalline cone (Land, 1981; Nilsson & Kelber, 2007).

Millipedes (Diplopoda) form a clade (Regier et al., 2010; Rehm, Meusemann, Borner, Misof, & Burmester, 2014) with more than 12,000 nominal species (Sierwald & Bond, 2007). They are predominantly night-active saprophagous, forest-dwellers, where they can be important consumers of leaf litter, and defend themselves via noxious secretions and a tough integument. In many species, lateral eyes are absent or consist of a few ommatidia, such as the pill millipede *Glomeris* (Munoz-Cuevas, 1984) or separate eye cups in the case of the basal Penicillata (Müller, Sombke, & Rosenberg, 2007). Millipedes typically have cryptic lifestyles and avoid light, including some eyeless species (Cloudsley-Thompson, 1951; Meyer-Rochow, 2015), although some are diurnal and others approach light while active at night.

Among several extant orders, the adult eye comprises more than 15 ommatidia (Blanke & Wesener, 2014) forming a convex lattice extending from the dorsolateral to the dorsal part of the head, posterior to the antenna. Each ommatidium consists of a corneal lens, corneagenous cells, photoreceptor cells and pigment cells. The eye grows incrementally via the addition of new ommatidial rows (eyerows) at subsequent moults, beginning with a single posterolateral ommatidium at the second moult and expanding anteriorly. In comparison with anatomy, little is known of the physiology or function of millipede eyes (Müller & Sombke, 2015).

The aim of the present work is to measure the spatial resolution of millipedes. To investigate the performance of this eye-type, we carried out behavioural assays of spatial resolution of the eye of the julid millipede *Cylindroiulus punctatus* (Leach, 1815). The Julidae is a family of cylindrical millipedes mostly found in the western Palaearctic. It is abundant in northern European forests and gardens, where it is found in and under logs, among leaf litter and in the humic and mineral layers of soil, with their relative abundance in these microhabitats shifting over the course of the year (Banerjee, 1967). *C. punctatus* is a typical member

* Corresponding author.
E-mail address: john@jkirwan.org (J.D. Kirwan).

https://doi.org/10.1016/j.visres.2019.09.003
Received 19 February 2019; Received in revised form 3 September 2019; Accepted 18 September 2019
Available online 14 October 2019

of the Julidae in its general bauplan and regarding the structure of its eye. It lives over two years, developing in twelve stadia but lingering mostly in the final three as sexually mature adults (Saudray, 1952), during which the eye continues to grow. Maturity can occur earlier (Blower & Gabbutt, 1964) and as many as 14 stadia are reported (Enghoff, Dohle, & Blower, 1993).

We use a multilevel logistic regression model computed using Bayesian inference to help characterize the uncertainty of this detection task. Specifically, we find a detection threshold by modelling the psychometric function: a means of quantifying performance of spatial resolution, which is applied to stimulus perception by humans (Knoblauch & Maloney, 2012, pp. 107–140). We chose this approach because it incorporates all the data, including individual variation, in a joint model, and Bayesian estimation performs well with generalized nonlinear models.

We computed the angular sensitivity necessitated by this resolution. In addition, we investigate optically-important features of the eye anatomy and relate these to our behavioural measurements. We find that *C. punctatus* has coarse resolving vision, equivalent to a photoreceptor acceptance angle of 72°, assuming a contrast threshold of 10%, based on its orientation behaviour. This vision could be used to find shelter or avoid large obstacles during foraging or when disturbed.

2. Methods

2.1. Collection and husbandry

Adult millipedes were collected in Skåne, Southern Sweden from the following localities: 55°42′49.5″N 13°12′24.5″E, 56°05′02.4″N 13°14′00.9″E, 55°41′26.9″N 13°21′45.2″E and 55°43′37.0″N 13°06′23.9″E between March and December 2017 and in May 2019. Individuals of several species were initially collected and tested for their behavioural response to light. *C. punctatus* (Fig. 1A) was chosen for further experiments because it responsed to a printed visual stimulus (see below) and it could be readily collected and cared for. Animals were housed individually in petri dishes half-filled with 1% non-nutrient agar with a decaying deciduous leaf (typically *Corylus avellana* L. or *Fagus sylvatica* L.) at 14–20 °C on a 12:12 h light:dark cycle.

2.2. Eye anatomy

To give an overview of the eye morphology of *C. punctatus* and measure important attributes as a compliment to behavioural analyses, we carried out electron microscopy, light microscopy and X-ray microtomography (μCT) on the eyes of several animals used in the behavioural trials. Six individuals were sacrificed for imaging by excision of the head, collum and foremost segments (Fig. 1A). Antennae were partly removed to facilitate fixation. The heads were then promptly placed in 1.5 mL fixative solution and left overnight at 4 °C. The fixative comprised 2.5% glutaraldehyde; 2% paraformaldehyde and 2% sucrose in 0.1 M phosphate buffer. The samples were then washed repeatedly in buffer and post-fixed in 1% osmium tetroxide within buffer for 2 h and rewashed. They were then dehydrated in an ethanol series, rinsed with acetone, pre-embedded in Epon for over 12 h, and embedded in fresh Epon, which was polymerized for 48 h at 60 °C. A further six individuals were sacrificed as above but directly dehydrated in an ethanol series and critical point dried. Of these, two heads (one each from a male and a female) were then sputtered with gold for scanning electron microscopy, which with carried out with a Hitachi (Tokyo) SU3500 microscope.

Four additional samples were dried, as above, and used for μCT. These samples (three adults and one juvenile) were not sputtered but were glued to clear acrylic mounts and scanned at 80 kV using a Zeiss Xradia XRM520 (Carl Zeiss Microscopy GmbH, Jena, Germany). They were imaged at 1.4 μm resolution at 80 kV for a total of 997 projections (630 for the juvenile). Reconstruction of μCT images was carried out using Amira 6.4 (FEI, Hillsboro, OR, USA) and used to visualize and measure the cuticle, including the cuticular cornea, which shattered during TEM sectioning. All preparations were performed in a lit environment.

Image measurements were made using FIJI image analysis software (Schindelin et al., 2012; Schindelin, Rueden, Hiner, & Eliceiri, 2015) or within Amira. We imaged the high contrast cuticle to the exclusion of proximal elements of the eye. Any manipulations which were made to images were applied generally and not to specific areas. Imaging of transverse TEM sections through ommatidia were used to measure retinula depth and width as well as the facet diameter. Inter-ommatidial angles ($\Delta\phi$) were measured from a μCT model as was the radius of curvature of the facet (from averaging 20 fitted circles using the raw images). By assuming a homogenous refractive index profile of the cornea above the ommatidium, the optical acceptance angle ($\Delta\rho$) of an ommatidium could be estimated from morphology. The nodal point was assumed to be at the centre of curvature and the angle was found between this point and the edges of the retinula, using the mean retinular width and corneal depth.

2.3. Behavioural setup

The behavioural setup (Fig. 1B) is similar to that described by Kirwan et al. (2018) but makes use of adapted visual stimuli as well as illumination and recording systems. Experimental trials were conducted in an arena comprising a cylinder of poster paper, enclosed by opaque black paper atop a wooden base. The cylinder was 50 cm in internal diameter of 50 cm and 60 cm in height. Above the arena, two Radion xr30w aquaria LED lights (Ecotech, USA) were fixed to produce an array of four equidistant clusters of LEDs resulting in broad-spectrum visible illumination. The diffuser comprised two sheets of 3/4 diffusion paper (Lee Filters 416, Andover, UK; transmission 50%, summed across 400–700 nm) sandwiched between two sheets of Makrolon® (Covestro, Germany) polycarbonate within a wooden frame.

2.4. Visual test patterns

The patterns consisted of rich black printed images, which were uniform in the vertical plane but in the horizontal plane included stimuli which consisted of dark (black) regions set against a lighter (grey) background. The signals used to compose the stimulus (Fig. 1C, D) were derived from a difference of Gaussians (DoG) function and are as described by Kirwan et al. (2018).

The side-welling radiance reflected from the patterns was measured within the complete setup with a calibrated TriOS Ramses spectroradiometer (TriOS, Germany), placed 5 cm from the arena wall. Background luminance was below 0.1 lx. The centre of the lens was raised 40 mm from the arena floor and parallel. Relative spectral irradiance (from 300 nm to 1200 nm, in 3 nm bins) of test pieces of material were measured in the arena setup with the same lighting regime. To determine the relative quantities of available light reaching the animal when reflected from differing ink shades, we used the relative spectral sensitivity of the centipede *Scutigera coleoptrata* L. (maximal sensitivity: 448 nm), measured electrophysiologically (Meyer-Rochow, Müller, & Lindström, 2006), as a proxy (lacking millipede data), which we fitted with a smoothing spline in MATLAB 9.1 (Mathworks, USA). We multiplied the spectral irradiance for each ink shade by this normalized spectral sensitivity curve and summed the resultant values for each ink

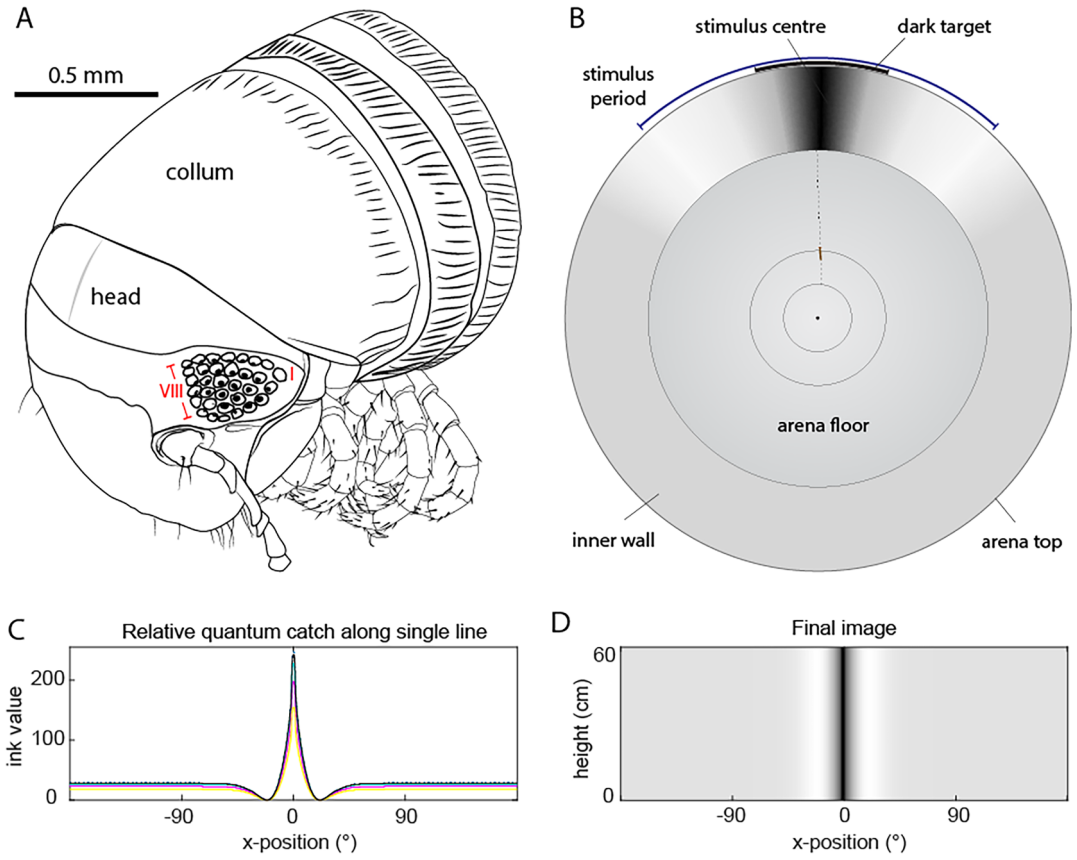

Fig. 1. The julid millipede *Cylindroiulus punctatus* and the experimental setup. (A) Diagram of the head and foremost segments of a *C. punctatus* adult female. I and VIII refer to the oldest (posterolateral) and youngest (anterodorsal) eyerows of the left lateral compound eye, respectively. (B) The experimental setup, viewed from the position of the camera, atop the arena. A millipede (brown) is indicated as well as the directional vector in relation to the arena wall. The arc width of the stimulus period (85°) and dark target are indicated by blue and black bars respectively. (C) Derivation of the 42° difference of Gaussians stimulus from printed CMYK ink values used in these behavioural assays. (D) Approximation of the final image based on these values. x-position refers to the angular distance from the midpoint of the stimulus target. (For interpretation of the references to colour in this figure legend, the reader is referred to the web version of this article.)

shade of ten samples of shaded paper of 12.5 cm^2 (0, 5, 10, 20, 30, 40, 50, 65, 80, 100%). We normalized these to the highest value to get relative available irradiances for each shade, then modelled changes in available light relative to ink value and printed the patterns accordingly (Fig. 1C, D).

2.5. Behavioural trials

Trials were conducted during the day phase of the animals' circadian entrainment at 22 °C and animals were kept in their described living conditions until shortly before trials. Trials were conducted individually, and the animal was coaxed by contact into fully coiling into a short helix (tighter than a flat spiral), obscuring their eyes, and placed onto the centre of the arena floor (Fig. 1B). The cylindrical walls and diffuser were then moved into position and the camera and lights readied. Trials only initiated if the animal fully coiled and remained in this position at the area centre during preparations (as it was observed in preliminary trials that animals would otherwise ignore even large stimuli). Between trials, the floor was brushed and wiped with ethanol – more extensively if the animal noticeably produced secretions. In each trial, the animal was placed by hand in the centre of the arena and allowed to move to the periphery. Trials lasted 5 min or until the animal approached the arena wall, if earlier. The walls and stimulus were rotated 90° clockwise for each subsequent trial, to negate other directional cues.

2.6. Recording and tracking

The trials were recorded using a Pi NOIR camera V2 controlled from a Raspberry Pi 3 model B (Raspberry Pi foundation, U.K.) with Python 3.6.3. The camera was positioned centrally above the arena (fixed to the LED clusters). The camera field of view included the arena floor and parts of the walls, including part of the stimulus. Videos were recorded at 1 fps, with a resolution of 960 × 720 pixels. To calibrate the recordings to account for image distortion, images were taken of a checkerboard pattern on the arena floor in many orientations. The subsequent images were calibrated using the camera calibration toolbox (Bouguet, 2004) within MATLAB. To provide a metric of probable orientation towards the stimulus or otherwise, individual animal paths were tracked as per Kirwan et al. (2018). Tracking was performed using custom software (Smolka et al., 2012) within MATLAB. To represent the bearing taken by the animal from the centre of the arena, the vector of the tracked points which were closest to one quarter and one half of the arena radius from the centre was determined, and the intersection of this vector with the arena wall was recorded. The angular position of this intersection point on the arena wall was used as a measure of the animal's bearing and this was determined in relation to the stimulus' position, i.e. moving in a straight

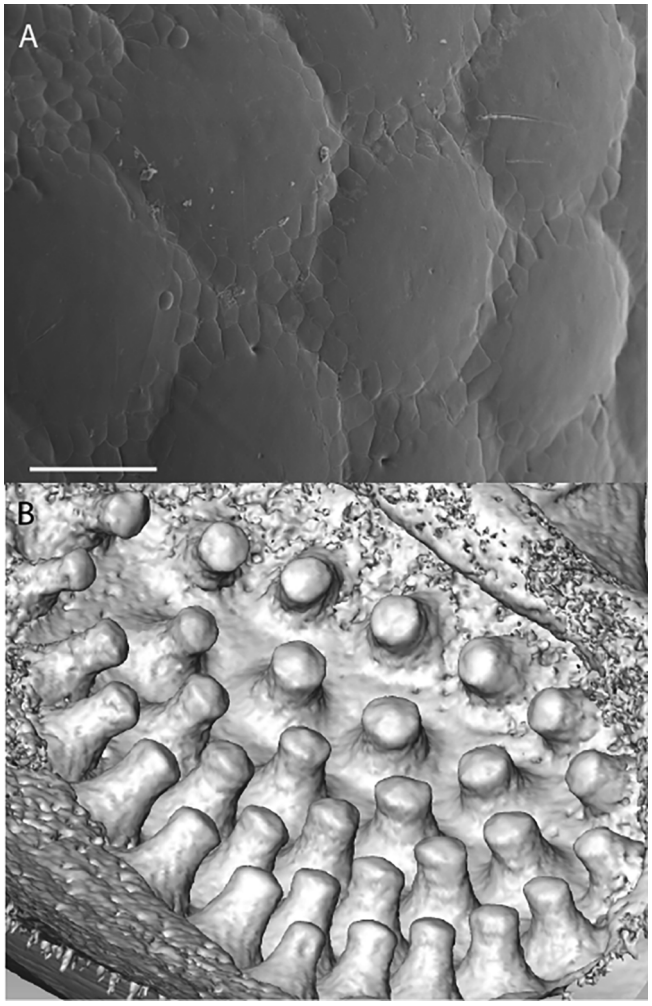

Fig. 2. Ultrastructure of the eye. (A) Scanning electron micrographs of ommatidial facets of the right eye of a *C. punctatus* adult (stadium IX) female. (B) Segmented μCT image showing the underside of the cuticular ommatidial lenses of the same individual. The head is intact and the cuticular cornea is visible given its high contrast, whereas the pigment layer and retina are not. The youngest eyerow comprising a single ommatidium is situated at the top left, and the oldest is on the bottom right. Scale bar: 25 μm.

line from the centre to the stimulus would correspond to a heading of 0 rad (0°) and the opposite orientation would correspond to π radians (180°). A trial was deemed completed if the animal moved at least 35% of the radial distance between the centre and arena walls.

2.7. Statistical analysis

To determine whether the taxis response varied as a function of the arc width of the stimulus, we defined a binomial success criterion for the observed data. This was done in preference to the angular data as we were concerned primarily with whether animals oriented to the target, rather than the precise heading. As a metric for response rate, we assessed success or failure in orientation for each trial by whether the bearing fell within a sector subtending 60° with the stimulus' centre at its arc midpoint (the target sector). This arc width was chosen to be slightly wider than the half-width of the widest stimulus applied and thus representative of which animals successfully oriented towards the stimulus.

For comparison, we computed the results of the Rayleigh test and V-test for each treatment, which, respectively, test for circular clustering in general and assuming a bias towards a prespecified direction (Batschelet, 1981, pp. 54–60). We also computed the results of a binomial test for each treatment, which tested the hypothesis that the proportion of animals directed towards the target sector should be equivalent to or less than would be expected by chance for disoriented animals. These analyses were carried out using R (R Core & Team, 2017). Alpha was 0.05 for all null-hypothesis tests.

To estimate the detection threshold, we implemented a Bayesian inference model using the Stan language (Carpenter et al., 2017) via the *brms* package (Bürkner, 2017) within R. We used a mixed-effects logistic regression model to implement the psychometric function with estimated upper and lower asymptotes to represent the chance and lapse rates of the response respectively. We chose this modelling approach because it accounts for individual variation which can carry important information, it disregards statistical significance, over-reliance on which can be problematic (McShane, Gal, Gelman, Robert, & Tackett, 2017), and the use of Bayesian priors guards against separation in logistic regression (Gelman, Jakulin, Pittau, & Su, 2008) and allows for many parameters and nonlinear models to be estimated effectively.

The chance rate is the rate at which successful orientation occurs at random in disoriented animals and the lapse rate is that at which animals fail to respond to a maximally detectable stimulus of this type. The criterion used to define the estimate was the inflection point of the psychometric function curve. The psychometric function is a description of the relationship between performance (in this case, visual stimulus detection) and stimulus intensity (the arc width of the difference of Gaussians stimulus) (see Knoblauch & Maloney, 2012; Wichmann & Hill, 2001). This was used because it is a feature of the fitted curve and not dependent on the bounds of an arbitrary interval and is commonly used as a measure of detection threshold (i.e. it is a parameter of the fitted curve that is relatively robust to sample size). The psychometric function $\psi(x;\, \alpha,\, \beta,\, \gamma,\, \lambda)$ was formulated as:

$$\psi(x;\, m,\, w,\, \gamma,\, \lambda) = \gamma + (1 - \gamma - \lambda)\cdot\Phi(x;\, m,\, w) \quad (1)$$

following Houpt and Bittner (2018), where γ is the chance rate of the response and λ the lapse rate, represented by lower and upper asymptotes, respectively. $\Phi(x;\, m,\, w)$ is the joint distribution of parameters modelled according to a sigmoidal logistic function, where x is the stimulus size (arc width), m is the threshold of detection and w is the difference between the stimulus width which would produce 10% success versus that which would produce 90% success, if γ and λ were 0. The model is defined such that:

$$\Phi(x;\, m,\, w) \sim Bin(n_i,\, p_i) \quad (2)$$

$$logit(p_i) = \frac{4.39\cdot(x_i - m_i)}{w_i}$$

where *logit* is the logistic transformation, *Bin* is the binomial distribution with parameters n and p: sample size and probability, respectively. A random intercept for individual variation was estimated for each of γ, m and w to account for differences between animals. Informative priors were used: on the variance of the random intercepts and on λ to facilitate convergence, on x and w to favour a threshold in the range of stimulus sizes applied, on γ to constrain it close to the random probability of success (1/6). The model was run for 10,000 post-warmup iterations from four Markov chains and all posterior draws were

analysed.

We represented the model graphically by investigating the outcome of the stimulus arc width predictor. We plotted a best fit line and 95% credible interval (CI) of the marginal effects at the median of this effect to interpret the results. Credible intervals are a range of values of an effect into which a given percentage of model predictions lie and, in this case, represent a 95% probability that the effect is truly within this range, according to the model. To ensure that the fit of this model was better than a model for which increasing stimulus size did not predict increasing response, we compared these two using approximate leave-one out cross-validation (LOO) which evaluates out-of-sample prediction accuracy and is applicable to multilevel Bayesian models (Vehtari, Gelman, & Gabry, 2017).

2.8. Behavioural estimation of angular sensitivity

The detection tests allowed us to model a range of values within which the spatial resolution of the visual behaviour might fall, with respect to a plausible range of contrast threshold values. Having found the spatial resolution of *C. punctatus* for the stimulus, we estimated the angular sensitivity needed to achieve this by modelled stimulus visibility to photoreceptors of differing angular sensitivity, as described in Kirwan et al. (2018). Different sizes of stimulus were convolved with a Gaussian spatial filter and the modulation of the filtered image was calculated to find the contrast remaining. We found the narrowest receptor angle at which the remaining contrast dropped to a range of contrast threshold values. As detection depends on both spatial resolution and contrast, and contrast sensitivity data are unavailable, we assumed a range of contrast sensitivity, equivalent to a contrast threshold of 5–20%. This range was selected to be in the range of most birds and some insects but worse than the range evinced by many vertebrates and some insects.

3. Results

3.1. Eye morphology and optics

From μCT of three adults (two in stadium IX and one in stadium X) the eye comprised between 31 and 37 facets arranged in rows (Blanke & Wesener, 2014; Vachon, 1947) of 1 + 2 + 3 + 4 + 5 + 5/6 + 6 + 5/6 + 5 (Fig. 2). We found the mean facet diameter of both eyes to be 52.9 μm (± 7.6 μm, s.d.). Facets were widest in the posterolateral (oldest) two eyerows (mean: 56.3 μm ± 6.5 μm, s.d.) and tapered in size towards the anterodorsal (youngest) row (mean: 47.2 μm, ± 4.5 μm, s.d.). The peripheries of the facets are perforated by occasional pores (Fig. 2A). The facets of the younger (stadium VI) juvenile eye were smaller (mean: 43.5 μm ± 4.6 μm, s.d.). Further measurements of the cornea using μCT were derived from a single adult female. The depth of the corneal lens varied, with a mean of 119.8 μm (± 60.6 μm, s.d.). This is partly accounted for by a cone-shaped projection into each ommatidium, surrounded by corneagenous cells. These corneal cones are proximally truncated by a rounded inner surface abutting the rhabdom. Measurements of the retinula were made from light microscopic serial sections of four animals. The rhabdom was found to be 34 μm wide (± 10.8 μm, s.d.) and 15 μm deep (± 2.7 μm, s.d.).

The ommatidia are optically-isolated from each other and the surrounding tissue by the pigment layer (Fig. 3A, B), and the curved facets suggest it is a focal apposition eye, for which the curvature of the cornea provides refractive power. Within this layer, surrounding the cornea, is the layer of corneagenous cells. The brittle cuticle was mostly lost during sectioning but from the remaining sections, distinct layers can be observed (Fig. 3E). From cross-sections through the ommatidia we found the rhabdom to be formed by at least 35 retinular photoreceptor cells in this plane (Figs. 3C, D and S1), based on the presence of desmosomes at the boundary of the microvilli. The microvilli are not, however, highly ordered in perpendicular rows in cross-section, suggesting that millipedes cannot discriminate the plane of polarization of light. Nor is there clear spatial compartmentalization of the microvilli within the retinula, and thus no indication of spatial resolution within the ommatidium.

The inter-ommatidial angle (Δϕ) was in the range of 5.5°–20.6° for the measured facets. The mean Δϕ between the eight anterodorsal facets (eyerow VIII) of the eye was 15.5° (± 3.8°, s.d.), whereas the mean Δϕ across the six ventral ommatidia was 14.8° (± 4.8°, s.d.). The field of view of the eye (measured between the optical axes of the peripheral ommatidia) was 83° dorsoventrally (between the opposite ommatidia of the youngest eyerow) and 66° laterally (between the oldest eyerow and the ventral ommatidium of the youngest eyerow). The outer radius of curvature of the corneal facet was found to be 125.2 μm (± 40.3 μm, s.d.). Assuming a nodal point at the centre of curvature of the corneal surface, the diameter of the rhabdom would generate acceptance angles of about 30°. The mean inter-ommatidial angle measures from the micrographs was 22.5° (± 3°, s.d.), within the range of the μCT measurements.

3.2. Behavioural experiments – object taxis

A total of 340 trials were completed from 68 *C. punctatus* individuals (summarized in Table 1; detailed in Table S1), which met the conditions of the assay, i.e. animals left the arena central region. The number of successful trials (e.g. Movie 1) per stimulus condition ranged between 33 and 52 (mean = 42.5 ± 5 6, s.d.). Each animal succeeded in at least one trial. In the circular scatter plots of the data (Fig. 4), animals are clearly oriented in the treatments associated with the widest two stimuli (113° and 141°), also apparent from the mean resultant length (ρ), a measure of circular concentration, and supported by the null hypothesis tests (Table 1). The narrowest three treatments, 0° (negative control), 14° and 28° are disoriented.

Movie 1.

The three intermediate stimulus treatments: 42°, 56° and 85° are more equivocal. The 42° treatment shows a concentration of animal headings towards the stimulus target which is significant according to the binomial and V-tests. The 56° treatment shows evidence of orientation only according to the binomial test. For the 85° treatment, headings are concentrated towards the stimulus, which is supported by the binomial and V tests. It should be noted that the angles here given are for the stimulus period and that the dark target area to which animals are attracted is much smaller (approximately 35% of the period) (Fig. 4).

3.3. Multilevel logistic regression model

The logistic regression model applied here estimates spatial

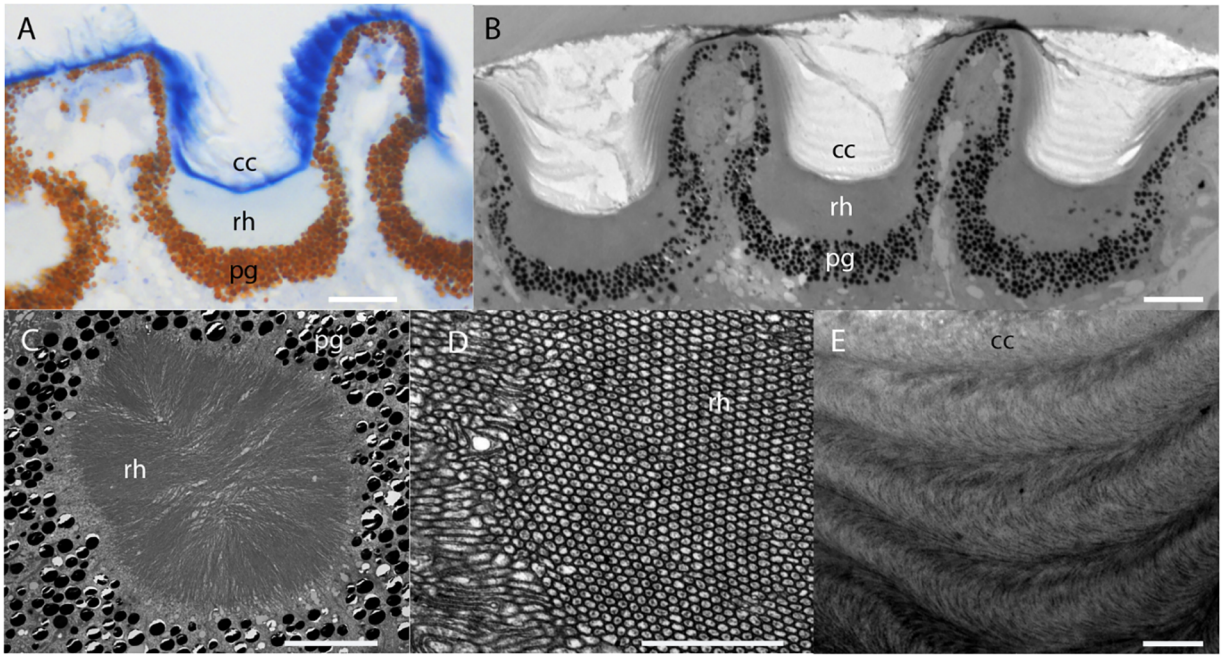

Fig. 3. The julid millipede *Cylindroiulus punctatus* ommatidial structure. (A) Light micrograph of ommatidium longitudinal section; cuticule is mostly absent, having shattered upon sectioning; (B–E) Transmission electron microscopy (TEM) sections through ommatia. (B) Longitudinal sections through ommatidia; (C) Rhabdom in cross-section; (D) Detail of retinular microvilli; (E) Cornea showing layered cuticular structure. *Abbreviations:* pg = pigment granules, rh = rhabdom, cc = corneal cone. Scale bars: A, B: 10, μm, C: 5 μm, D, E: 1 μm.

resolution based on the relative success of animals approaching the dark target of the stimulus over many trials for differing stimulus widths. For the given model, the Bayesian process estimates the probability at which a specific value of each the model parameters could have resulted in the observed data (the posterior probability). It provides both an estimate of spatial resolution and a meaningful expression of the uncertainty. Four independent chains are used to ensure that the entire posterior distribution is explored. The model converged without divergent transitions, according to visual inspection of the Markov chains (Fig. S2), statistical checks (Gelman and Rubin (1992) convergence statistic = 1 and neff/N > 0.4 for each parameter) and a posterior predictive check (Fig. S3). The model fit outperformed an alternative model that excluded stimulus arc width as a predictor (LOO values differed by 15.0, s.e.m. 4.5). The diagnostics support the validity of the model.

We investigated the marginal effect at the median for the effect of stimulus period, conditioned upon the remaining parameters. The resulting representation of object taxis response to the stimuli (Fig. 5) indicates that the most probable chance rate (random probability of success) is 0.165 (95% CI: 0.08–0.24) and lapse rate (failure rate when the stimulus is maximally detectable) is 0.47 (95% CI: 0.40–0.55) (Table S1). We found the detection threshold (Fig. 5) to occur at 56° (95% CI range: 37°–82°). The observed proportion of successful orientations per treatment falls outside the 95% CI for two treatments (113°) even when incorporating the effect of individual, indicating that this high proportion is less plausible according to the model.

Applying the median estimate of the detection threshold at which *C. punctatus* could resolve the difference of Gaussians stimulus (56°), we found the maximum acceptance angle which could achieve this resolution (Fig. 6) to be in the range: 52°–97° assuming a contrast threshold between 5% and 20%, and 72° assuming a contrast threshold of 10%.

4. Discussion

4.1. Millipedes have extremely low-resolution vision

The spatial resolution exhibited by *C. punctatus* in our experiments limits vision to a narrow range of tasks, including the dark object taxis displayed in our experiments. This task has an obvious application to shelter-seeking, helping these animals to find the logs, litter or soil layers which constitute their dwellings and the source of their

Table 1
Summary of taxis behavioural experiments. Treatment arc refers to the arc with of the stimulus period for each of the eight stimulus treatments, including the control (0°). Test statistics (where appropriate) and p-values are reported for three null-hypothesis tests (α = 0.05); significant values are indicated with an asterisk (*).

Stimulus period arc width (°)	n	Correct (%)	V test statistic	p-value	Rayleigh test		Binomial test
					statistic	p-value	p-value
0	47	17	−0.03	0.600885	0.04	0.929635	0.534446
14	41	22	0.10	0.171676	0.17	0.288110	0.234994
28	44	16	−0.19	0.962725	0.23	0.106863	0.616075
42	42	42	0.25	0.012325*	0.25	0.080645	0.000152*
56	42	29	0.01	0.454381	0.16	0.341723	0.037629*
85	52	38	0.17	0.038537*	0.17	0.208242	0.000143*
113	33	66	0.61	2.0×10^{-7}*	0.61	0.000002*	8.8×10^{-10}*
141	39	59	0.45	0.000029*	0.45	0.000245*	3.0×10^{-9}*

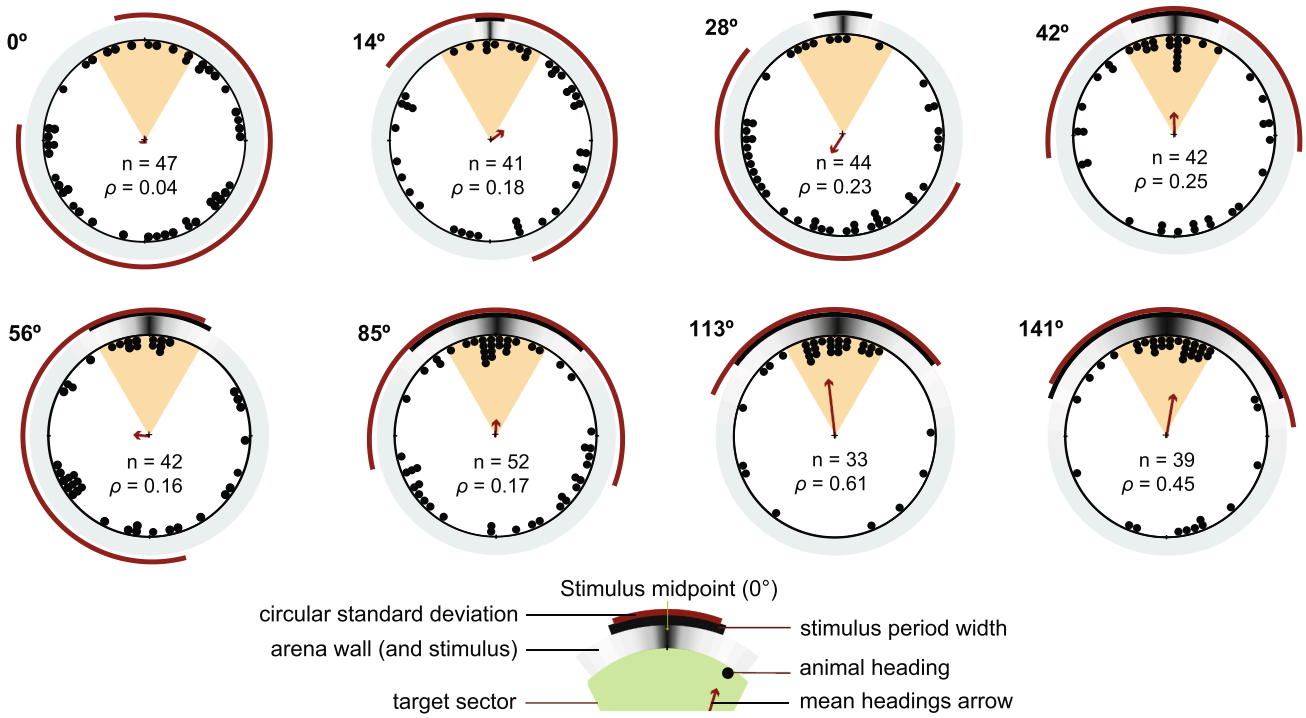

Fig. 4. Circular plots of the direction taken by *C. punctatus*. The large circles are scatter plots of directional vectors taken by millipedes from the circular centre for each trial. Each circle represents a different arc width of the stimulus period. The mean heading arrow (red) points towards the circular mean of the observations for that condition and the length of the arrow relative to the arena represents the mean resultant length (ρ). The red arc represents the circular standard deviation. The green sector indicates the target sector; trials for which the animal oriented towards this sector were counted as successful orientations. (For interpretation of the references to colour in this figure legend, the reader is referred to the web version of this article.)

herbaceous food. At this resolution, a millipede could resolve a 1 m wide log from 2.9 m away (see Fig. 7).

Lacking an observable visual looming response, shelter-seeking may constitute the main visually-guided behaviour in this species. This behaviour is unlikely to contribute to predator evasion because high contrast objects must exceed 20° to be detected, implying that approaching predators, such as rove beetles or the hedgehog, *Erinaceus europeaus*, (David, 2015), are seen only after reaching striking distance. Similarly, the poor spatial resolution precludes detection of conspecifics beyond the ranges of touch and smell. Most millipedes are not highly social and primarily interact with conspecifics to mate, although some species, including *C. punctatus*, may aggregate together with conspecifics. Nonetheless, there are social species, which exhibit parental care (Kudo, Akagi, Hiraoka, Tanabe, & Morimoto, 2011) and mass aggregations (Meyer-Rochow, 2015). It appears unlikely that low-resolution vision like that found here, could play any significant role in social behaviour.

The ommatidia of the *C. punctatus* eye are likely the spatial sampling units, given the rhabdom morphology with no shielding between contributions from different receptor cells. In addition, the behaviourally-inferred acceptance angle ($\leq 72°$) exceeds that estimated from anatomy (30°) for the entire rhabdom.

Other photodetectors occur in millipedes beyond the compound eyes. Accessory lateral eyes, cerebral photosensitive organs connected to the optic neuropil, are present in some millipede species, having been identified in *Cylindroiulus truncorum* (Heithier & Melzer, 2005). In *C. truncorum* they include six photoreceptor cells and supporting cells but appear to lack focusing optics. *Chamberlinius hualiensis*, an eyeless polydesmid that undergoes mass migrations, is strongly negatively phototactic, and this may be mediated by cerebral photoreceptors (Meyer-Rochow, 2015). However, such a system could not mediate visual behaviours such as the object taxis elicited in these experiments. *Cylindroiulus* species and others which are equipped with lateral compound eyes could use accessory lateral eyes for the simpler tasks such as maintaining endogenous rhythms or simple phototaxis.

Millipedes utilise other sensory modalities to perceive their environment. The antennae, which continuously probe the substrate as the animal moves, have a role in both mechanoreception and chemoreception and several sensory sensilla have been described in the antennae of *C. punctatus* (Müller & Sombke, 2015). Close to the antennae are the organs of Tömösváry, which may have a role in chemoreception. The low-resolution vision of *C. punctatus* could augment the sensory repertoire of this species by the addition of, otherwise unavailable, long-range instantaneous information (e.g. the location of a shelter, or the way out from a shelter). The generality of the myriapod eye design among several orders of Chilognatha makes *C. punctatus* a reasonable model for many diplopods.

The taxis response of *C. punctatus* may underexploit the maximum performance of the visual system. Animals might detect smaller stimuli but be unmotivated to respond to the stimuli under the conditions provided or in the current behavioural states. Spatial filtering of visual information could also occur, which would make specific spatial frequencies more salient or attractive in contrast to the monotonic increase in response presumed by the psychometric function.

While facet diameters vary enormously in millipedes, they are large (see Müller & Sombke, 2015), often dwarfing those of insects, which is

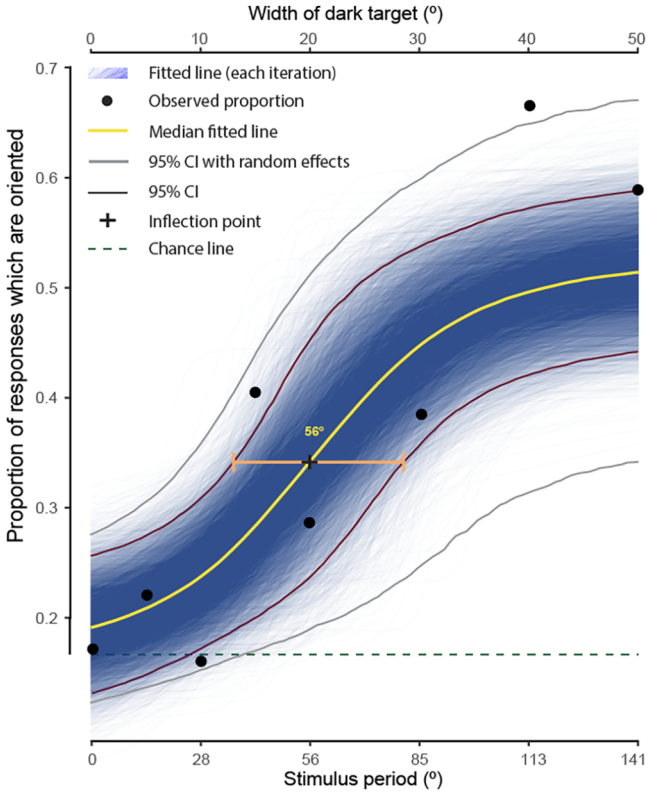

Fig. 5. Psychometric function of response to visual stimulus. The plot represents the marginal effects at the median of the effect of stimulus period, conditioned upon the remaining parameters. The black dots (●) represent the proportion of successful orientations at each treatment. The estimate of the detection threshold is 56° (95% Cl range: 37°–82°). The grey and black lines represent the 95% credible intervals (CI) with and without random intercepts for individual variation respectively. Fitted line (each iteration) represents the fitted line drawn from the posterior values for 10,000 iterations across the four Markov chains.

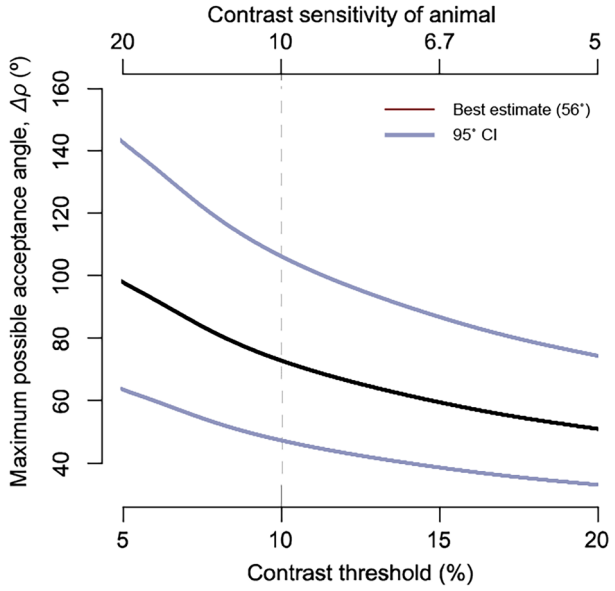

Fig. 6. Angular sensitivity of the millipede *Cylindoiulus punctatus*. We calculated the maximum possible acceptance angle of the visual system which could detect a given stimulus size. As detection is dependent on both resolving power (angular sensitivity) and contrast sensitivity and as the contrast sensitivity is unknown, these ranges were estimated across an ecologically plausible range of contrast threshold values (5–20%). This was calculated by simulating the change in contrast over the stimulus, with decreasing visual acceptance angle for a series of contrast threshold values. We assume a Gaussian acceptance function and calculate the signal modulation when the acceptance function is scanned across a target of 56° period arc width. Contrast threshold is the reciprocal of contrast sensitivity, expressed as a percentage (Michelson contrast). The upper and lower bounds of each range were calculated by simulating the change in contrast over the stimulus, with decreasing visual acceptance angle for a series of contrast threshold values. This was done for the 95% credible intervals of the resolution estimate. At an assumed contrast threshold of 10%, the theorized acceptance angle of this animal is 72°.

consistent with sensitive, low resolution vision. The dismal spatial resolution and the sluggish locomotion of the animal (which facilitates light sensitivity) suggest that the eye is adapted for visual tasks performed under dim light.

As the size of eye and number of ommatidia varies between and within the stages of the adult millipede, it would be intriguing to investigate if these differences are associated with differential visual performance. The growth of fewer ommatidia in the eye rows than would ideally be expected by row number in julids (referred to as reduction of the field) varies markedly between species and depending on eye shape (Enghoff et al., 1993). Sahli (1955) found a difference in this reduction between individuals of *C. punctatus*, with more subterranean individuals more reduced.

By modelling the psychometric function using a Bayesian mixed-effects model, we have been able to estimate resolution even with a large lapse rate (failure rate in case of a salient stimulus) which can confound other statistical approaches.

4.2. Conclusions

We find that *C. punctatus* can resolve a difference of Gaussian stimulus of 56° period width (20° half width of central dark bar). This calls for a theoretical acceptance angle no wider than 72° assuming a contrast threshold of 10%, based on measured behavioural thresholds. The acceptance angle estimated from ommatidial anatomy is approximately 30°, and the interommatidial angles range from about 5°–21°.

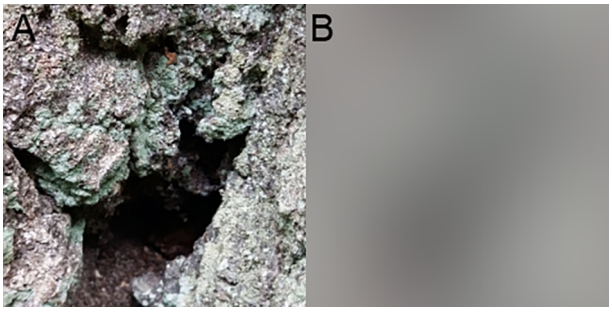

Fig. 7. Visual acuity of the millipede *C. punctatus*. To represent the acuity provided by *C. punctatus* vision, an image was blurred using the AcuityView package (Caves & Johnsen, 2018) in the R environment. An acceptance angle of 72° was used based on the ability to resolve a difference of Gaussians pattern of 56° (see Section 3.3). A crevice at the base of a tree (A) from 1 cm is visible in B.

Declaration of Competing Interest

The authors declare that they have no known competing financial interests or personal relationships that could have appeared to influence the work reported in this paper.

Acknowledgements

We thank Sam Walmsley for his assistance with preliminary experiments, Henrik Enghoff for invaluable advice on millipede collection and husbandry, Ullrika Sahlin for assistance with Bayesian statistical procedures, Paul Bürkner for developing the 'brms' package and for his advice on its usage, James Foster for assistance with statistical analysis, James Foster and Almut Kelber for helpful feedback, Gavin Taylor, Pierre Tichit and Stanley Heinze for assistance with Amira, Carina Rasmussen for sectioning eyes and advice on fixation, Ola Gustafsson for assistance with electron microscopy and the Lund 4D lab for microtomography.

Funding

This project was funded by the Knut and Alice Wallenberg Foundation ('Ultimate Vision' to DEN) and by the Swedish Research Council (grant to DEN).

Appendix A. Supplementary data

Supplementary data to this article can be found online at https://doi.org/10.1016/j.visres.2019.09.003.

References

Banerjee, B. (1967). Seasonal changes in the distribution of the millipede *Cylindroiulus punctatus* (Leach) in decaying logs and soil. *The Journal of Animal Ecology, 36*(1), 171. https://doi.org/10.2307/3020.

Batschelet, E. (1981). *Circular statistics in biology*. New York: Academic Press.

Blanke, A., & Wesener, T. (2014). Revival of forgotten characters and modern imaging techniques help to produce a robust phylogeny of the Diplopoda (Arthropoda, Myriapoda). *Arthropod Structure & Development, 43*(1), 63–75. http://www.sciencedirect.com/science/article/pii/S1467803913000868.

Blower, J. G., & Gabbutt, P. D. (1964). Studies on the millipedes of a Devon oak wood. *Proceedings of the Zoological Society of London, 143*, 143–176.

Bouguet, J.-Y. (2004). Camera calibration toolbox for matlab. *Jean-Yves Bouguet's Homepage*. http://www.vision.caltech.edu/bouguetj/.

Bürkner, P.-C. (2017). brms: An R package for Bayesian multilevel models using stan. *Journal of Statistical Software, 80*(1), 1–28. https://doi.org/10.18637/jss.v080.i01.

Carpenter, B., Gelman, A., Hoffman, M. D., Lee, D., Goodrich, B., Betancourt, M., ... Riddell, A. (2017). *Stan*: A probabilistic programming language. *Journal of Statistical Software, 76*(1), 1–32. https://doi.org/10.18637/jss.v076.i01.

Caves, E. M., & Johnsen, S. (2018). AcuityView: An R package for portraying the effects of visual acuity on scenes observed by an animal. *Methods in Ecology and Evolution, 9*(3), 793–797. https://doi.org/10.1111/2041-210X.12911.

Cloudsley-Thompson, J. L. (1951). On the responses to environmental stimuli, and the sensory physiology of Millipedes (Diplopoda). *Proceedings of the Zoological Society of London, 121*(2), 253–277. https://doi.org/10.1111/j.1096-3642.1951.tb00795.x.

David, J. (2015). Diplopoda – Ecology. In A. Minelli (Ed.). *Treatise on Zoology – Anatomy, Taxonomy, Biology – The Myriapoda II* (pp. 303–327). .

Enghoff, H., Dohle, W., & Blower, J. G. (1993). Anamorphosis in millipedes (Diplopoda)-the present state of knowledge with some developmental and phylogenetic considerations. *Zoological Journal of the Linnean Society, 109*(2), 103–234. https://doi.org/10.1111/j.1096-3642.1993.tb00305.x.

Gelman, A., Jakulin, A., Pittau, M. G., & Su, Y. S. (2008). A weakly informative default prior distribution for logistic and other regression models. *Annals of Applied Statistics, 2*(4), 1360–1383. https://doi.org/10.1214/08-AOAS191.

Gelman, A., & Rubin, D. B. (1992). Inference from iterative simulation using multiple sequences. *Statistical Science, 7*(4), 457–472. https://doi.org/10.1214/ss/1177011136.

Heithier, N., & Melzer, R. R. (2005). The accessory lateral eye of a diplopod, *Cylindroiulus truncorum* (Silvestri, 1896) (Diplopoda: Julidae). *Zoologischer Anzeiger – A Journal of Comparative Zoology, 244*(1), 73–78. http://linkinghub.elsevier.com/retrieve/pii/S0044523105000306.

Houpt, J. W., & Bittner, J. L. (2018). Analyzing thresholds and efficiency with hierarchical Bayesian logistic regression. *Vision Research, 148*, 49–58. https://doi.org/10.1016/j.visres.2018.04.004.

Kirwan, J. D., Bok, M. J., Smolka, J., Foster, J. J., Hernández, J. C., & Nilsson, D.-E. (2018). The sea urchin Diadema africanum uses low resolution vision to find shelter and deter enemies. *The Journal of Experimental Biology, 221*, jeb176271. https://doi.org/10.1242/jeb.176271.

Knoblauch, K., & Maloney, L. T. (2012). *Modeling psychophysical data in R*New York: Springer. https://doi.org/10.1007/978-1-4614-4475-6.

Kudo, S.-I., Akagi, Y., Hiraoka, S., Tanabe, T., & Morimoto, G. (2011). Exclusive male egg care and determinants of brooding success in a millipede. *Ethology, 117*(1), 19–27. https://doi.org/10.1111/j.1439-0310.2010.01851.x.

Land, M. F. (1981). Optics and vision in invertebrates. *Handbook of sensory physiology, VII/6B* (pp. 471–592). Berlin: Springer. https://doi.org/10.1007/978-3-642-66907-1_4.

McShane, B. B., Gal, D., Gelman, A., Robert, C., & Tackett, J. L. (2017). *Abandon statistical significance*. http://arxiv.org/abs/1709.07588.

Meyer-Rochow, V. B. (2015). New observations – with older ones reviewed – on mass migrations in millipedes based on a recent outbreak on Hachijojima (Izu Islands) of the polydesmid diplopod (*Chamberlinius hualienensis*, Wang 1956): Nothing appears to make much sense. *Zoological Research, 36*(3), 119–132. http://www.ncbi.nlm.nih.gov/pubmed/26018855.

Meyer-Rochow, V. B., Müller, C. H. G., & Lindström, M. (2006). Spectral sensitivity of the eye of Scutigera coleoptrata (Linnaeus, 1758) (Chilopoda: Scutigeromorpha: Scutigeridae). *Applied Entomology and Zoology, 41*(1), 117–122. https://doi.org/10.1303/aez.2006.117.

Müller, C. H. G., & Sombke, A. (2015). Diplopoda-sense organs. In A. Minelli (Ed.). *Treatise on zoology – Anatomy, Taxonomy, biology – the Myriapoda II* (pp. 181–235). .

Müller, C. H. G., Sombke, A., & Rosenberg, J. (2007). The fine structure of the eyes of some bristly millipedes (Penicillata, Diplopoda): additional support for the homology of mandibulate ommatidia. *Arthropod Structure & Development, 36*(4), 463–476. https://doi.org/10.1016/J.ASD.2007.09.002.

Munoz-Cuevas, A. (1984). Photoreceptor structures and vision in arachnids and myriapods. In M. A. Ali (Ed.). *Photoreception and vision in invertebrates* (pp. 335–399). Boston, MA: Springer US. https://doi.org/10.1007/978-1-4613-2743-1_10.

Nilsson, D.-E., & Kelber, A. (2007). A functional analysis of compound eye evolution. *Arthropod Structure and Development, 36*(4), 373–385. https://doi.org/10.1016/j.asd.2007.07.003.

R Core Team (2017). *R: A language and environment for statistical computing*. Vienna, Austria: R Foundation for Statistical Computing. https://www.r-project.org.

Regier, J. C., Shultz, J. W., Zwick, A., Hussey, A., Ball, B., Wetzer, R., ... Cunningham, C. W. (2010). Arthropod relationships revealed by phylogenomic analysis of nuclear protein-coding sequences. *Nature, 463*(7284), 1079–1083. https://doi.org/10.1038/nature08742.

Rehm, P., Meusemann, K., Borner, J., Misof, B., & Burmester, T. (2014). Phylogenetic position of Myriapoda revealed by 454 transcriptome sequencing. *Molecular Phylogenetics and Evolution, 77*, 25–33. https://doi.org/10.1016/j.ympev.2014.04.007.

Rota-Stabelli, O., Campbell, L., Brinkmann, H., Edgecombe, G. D., Longhorn, S. J., Peterson, K. J., ... Telford, M. J. (2010). A congruent solution to arthropod phylogeny: Phylogenomics, microRNAs and morphology support monophyletic Mandibulata. In: *Proceedings of the Royal Society B, 278*, 298–306. https://doi.org/10.1098/rspb.2010.0590.

Sahli, F. (1955). Presence en Sarre et contribution á l'etude du developpement post-embryonnaire de *Cylindroiulus (Aneuloboiulus) silvarum* Meinert, 1868 (Myriapoda, Diplopoda, Iulidae). *Ann. Univ. Sarav Sei, 4*, 151–164.

Saudray, Y. (1952). Developpement post-embryonnaire d'un Iulide indigene *Cylindroiulus (Aneuloboiulus) silvarum* Meinert. *Archives de zoologie expérimentale et générale, 89*, 1–14.

Schindelin, J., Arganda-Carreras, I., Frise, E., Kaynig, V., Longair, M., Pietzsch, T., ... Cardona, A. (2012). Fiji: An open-source platform for biological-image analysis. *Nature Methods, 9*(7), 676. https://doi.org/10.1038/nmeth.2019.

Schindelin, J., Rueden, C. T., Hiner, M. C., & Eliceiri, K. W. (2015). The ImageJ ecosystem: An open platform for biomedical image analysis. *Molecular Reproduction and Development, 82*(7–8), 518–529. https://doi.org/10.1002/mrd.22489.

Sierwald, P., & Bond, J. E. (2007). Current status of the Myriapod class Diplopoda (Millipedes): Taxonomic diversity and phylogeny. *Annual Review of Entomology, 52*(1), 401–420. https://doi.org/10.1146/annurev.ento.52.111805.090210.

Smolka, J., Baird, E., Byrne, M. J., El Jundi, B., Warrant, E. J., & Dacke, M. (2012). Dung beetles use their dung ball as a mobile thermal refuge. *Current Biology, 22*(20), R863–R864. https://doi.org/10.1016/j.cub.2012.08.057.

Vachon, M. (1947). Contribution à l'étude du développement post-embryonaire de *Pachybolus ligulatus* Voges. Les étapes de la croissance. *Annales de Sciences Naturelles, Zoologie, Série, 11*(9), 109–121.

Vehtari, A., Gelman, A., & Gabry, J. (2017). Practical Bayesian model evaluation using leave-one-out cross-validation and WAIC. *Statistics and Computing, 27*, 1413–1432. https://doi.org/10.1007/s11222-016-9696-4.

Wichmann, F. A., & Hill, N. J. (2001). The psychometric function: I. Fitting, sampling, and goodness of fit. *Perception and Psychophysics, 63*(8), 1293–1313. https://doi.org/10.3758/BF03194544.